Thermochimica Acta

Experimental determination of phase stability of the cubic L12 HfAl3-xZnx phase

--Manuscript Draft--

Manuscript Number:	TCA-D-24-00576R2
Article Type:	Full Length Article
Section/Category:	Others
Keywords:	Trialuminides; Thermodynamic and thermochemical properties; calorimetry; X-Ray Powder Diffraction
Corresponding Author:	Simona Delsante University of Genoa Department of Chemistry and Industrial Chemistry Genoa, Italy
First Author:	Simona Delsante, Professor
Order of Authors:	Simona Delsante, Professor
	G. Borzone
	N. Parodi, Researcher
	S. Guerrucci, PhD Student
Abstract:	The present study is devoted to the experimental investigation of the range of existence and of the heat of formation (ΔfH° at 300K) of the cubic L12–HfAl3-xZnx solid solution. A high-temperature direct drop calorimeter has been employed to synthesize and simultaneously determine the ΔfH° of several alloys along the HfZn3-HfAl3 section (25 at. % Hf) whereas X-Ray Powder Diffraction (XRPD) and Scanning Electron Microscopy (SEM) paired with an EDS (Energy Dispersive Spectrometer detector) have been employed to characterize the samples. The performed analysis confirmed that the ternary HfAl3-xZnx alloys were nearly single phase in the range 1 ≤ x ≤ 2.24 having the cubic L12 structure; this in turn help establish the trend of L12 lattice parameter (at room temperature) with composition. Thanks to the interpolation of our experimental data, the following values of ΔfH° (kJ/mol-atom at 300K) for the L12-HfAl3-xZnx were determined: -37.1±2.0 (HfAl0.8Zn2.2 corresponding to Hf25Al20Zn55 at. %), -41.7±2.0 (HfAl1.2Zn1.8 corresponding to Hf25Al30.0Zn45.0 at. %), -45.1±2.0 (HfAl1.5Zn1.5 corresponding to Hf25Al37.5Zn37.5 at. %) and -48.5±2.0 (HfAl1.8Zn1.2 corresponding to Hf25Al45.0Zn30.0 at. %). For two pertinent binary intermetallic phases, the following ΔfH° values (in kJ/mol-atom) at 300K have been obtained: -31.8±3.0 for HfZn3 (unknown structure) and -37.0±2.0 for HfAl3 (tetragonal DO23 – type structure).
Suggested Reviewers:	Adam Dębski Professor, Institute of Metallurgy and Materials Science PAS a.debski@imim.pl Expert in thermodynamics of metal systems
	Ales Kroupa Professor, Institute of Physics of Materials Czech Academy of Sciences kroupa@ipm.cz Expert in structure of Phases and Thermodynamics
	Philip Nash Professor, Illinois Institute of Technology nash@iit.edu Expert experimental determination and theoretical calculation of phase equilibria. Intermetallics, calorimetry.
Opposed Reviewers:	
Response to Reviewers:	

Università di Genova | DCCI
Dipartimento di Chimica e Chimica Industriale

Genoa, 30-09-2024

Dear Editor,

I am pleased to submit to your attention the revised version of the original article entitled "Experimental determination of phase stability of the cubic $L1_2$ $HfAl_{3-x}Zn_x$ phase" by S. Delsante, G. Borzone, N. Parodi and S. Guerrucci, to be published in the "*Thermochimica Acta*" Journal.

This version has been modified taking into account your further comments/corrections after the firsr revision.

We hope that this updated version of our work will deserve the publication in the "*Thermochimica Acta*" Journal.

This manuscript is original work, has not been published previously and is not under consideration for publication elsewhere. All authors and relevant authorities agree with its submission to "*Thermochimica Acta*" Journal.

Thank you very much for your kind attention.

Best regards,

Simona Delsante.

Prof. Simona Delsante, PhD
Università degli Studi di Genova
Dipartimento di Chimica e Chimica Industriale
Via Dodecaneso 31, 16146 Genova, Italy
Tel.+39 0103536160/Fax +39 0103625051
e-mail: simona.delsante@unige.it

Università di Genova | DCCI
Dipartimento di Chimica e Chimica Industriale

Genoa, 30-09-2024

Dear Editor,

We made the required changes on figure 6 and equations have been numbered.

Thank you very much for your kind attention and best regards,

Simona Delsante.

Prof. Simona Delsante, PhD
Università degli Studi di Genova
Dipartimento di Chimica e Chimica Industriale
Via Dodecaneso 31, 16146 Genova, Italy
Tel.+39 0103536160/Fax +39 0103625051
e-mail: simona.delsante@unige.it

Highlights

- $\Delta_f H°$ at 300 K of several $HfAl_{3-x}Zn_x$ alloys have been measured by H.T. calorimetry
- Calorimetric data have been validated by XRPD and SEM-EDS analysis
- The trend of $\Delta_f H°$ *vs.* x for the cubic $L1_2$ - $HfAl_{3-x}Zn_x$ phase has been obtained
- The range of existence of the cubic $L1_2$ - $HfAl_{3-x}Zn_x$ phase has been determined

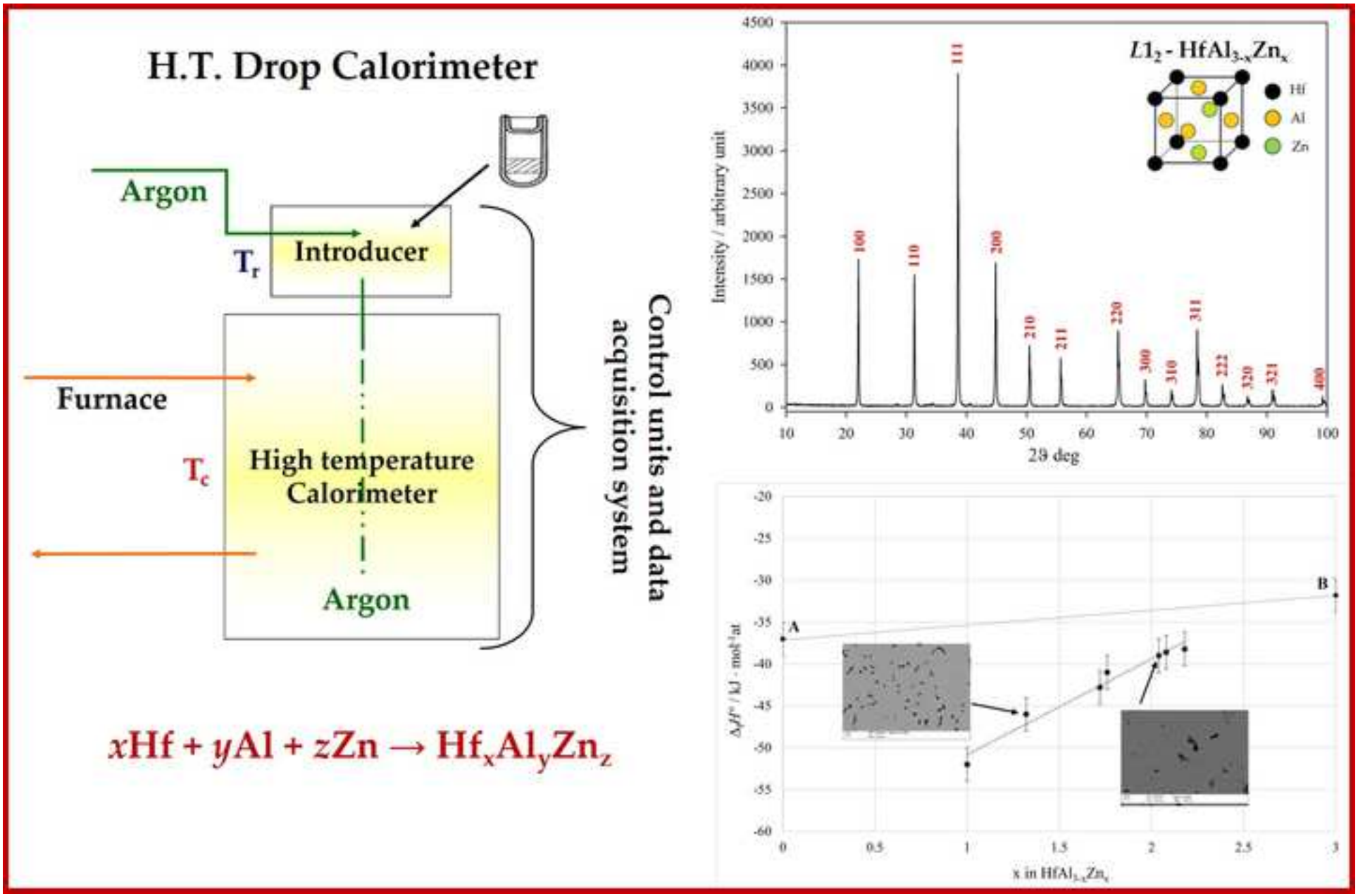

Figure

Click here to access/download;Figure;Figure_1_Delsante_Manuscript.tif

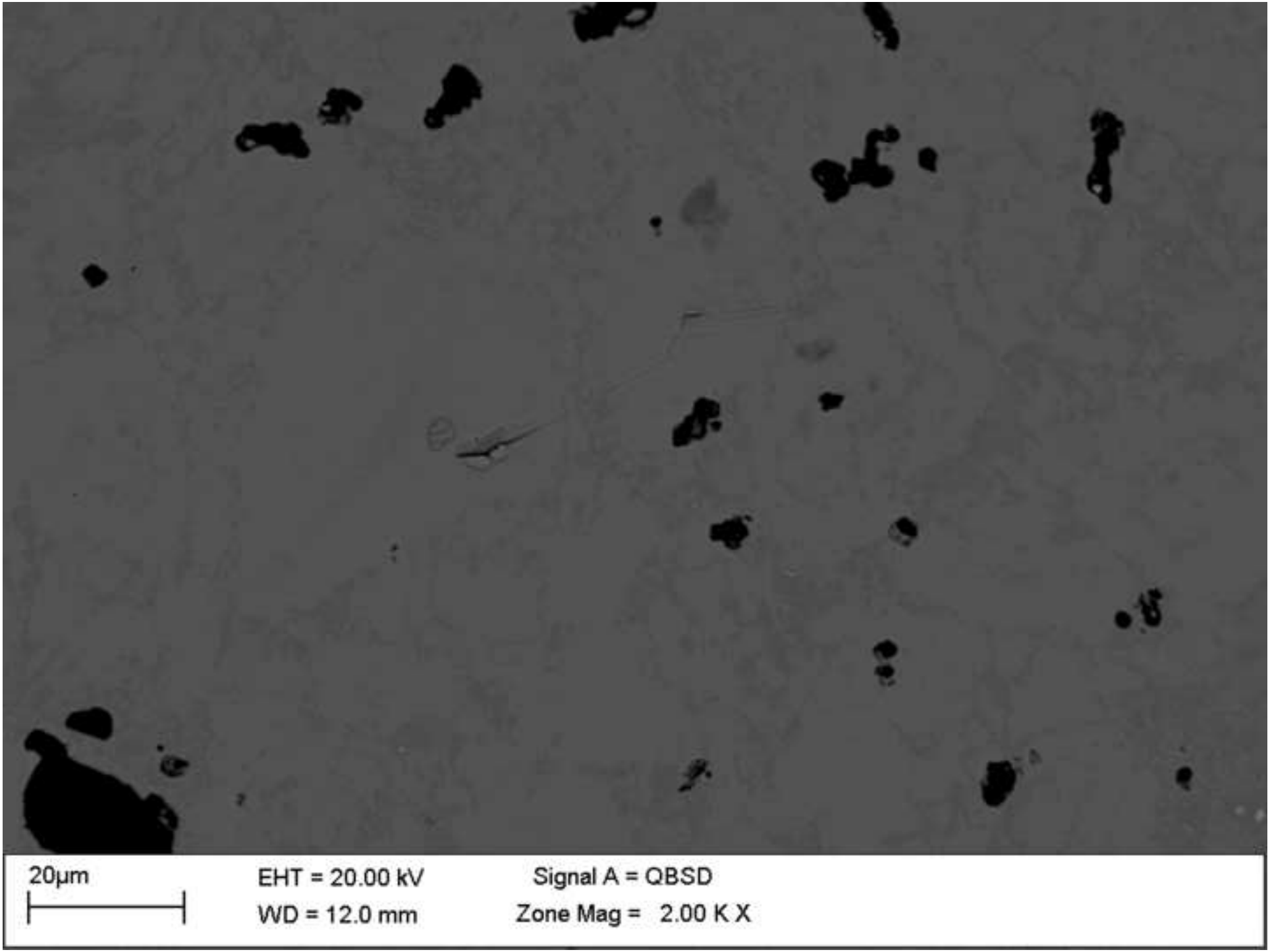

Figure

Click here to access/download;Figure;Figure_2_Delsante_Manuscript.jpg

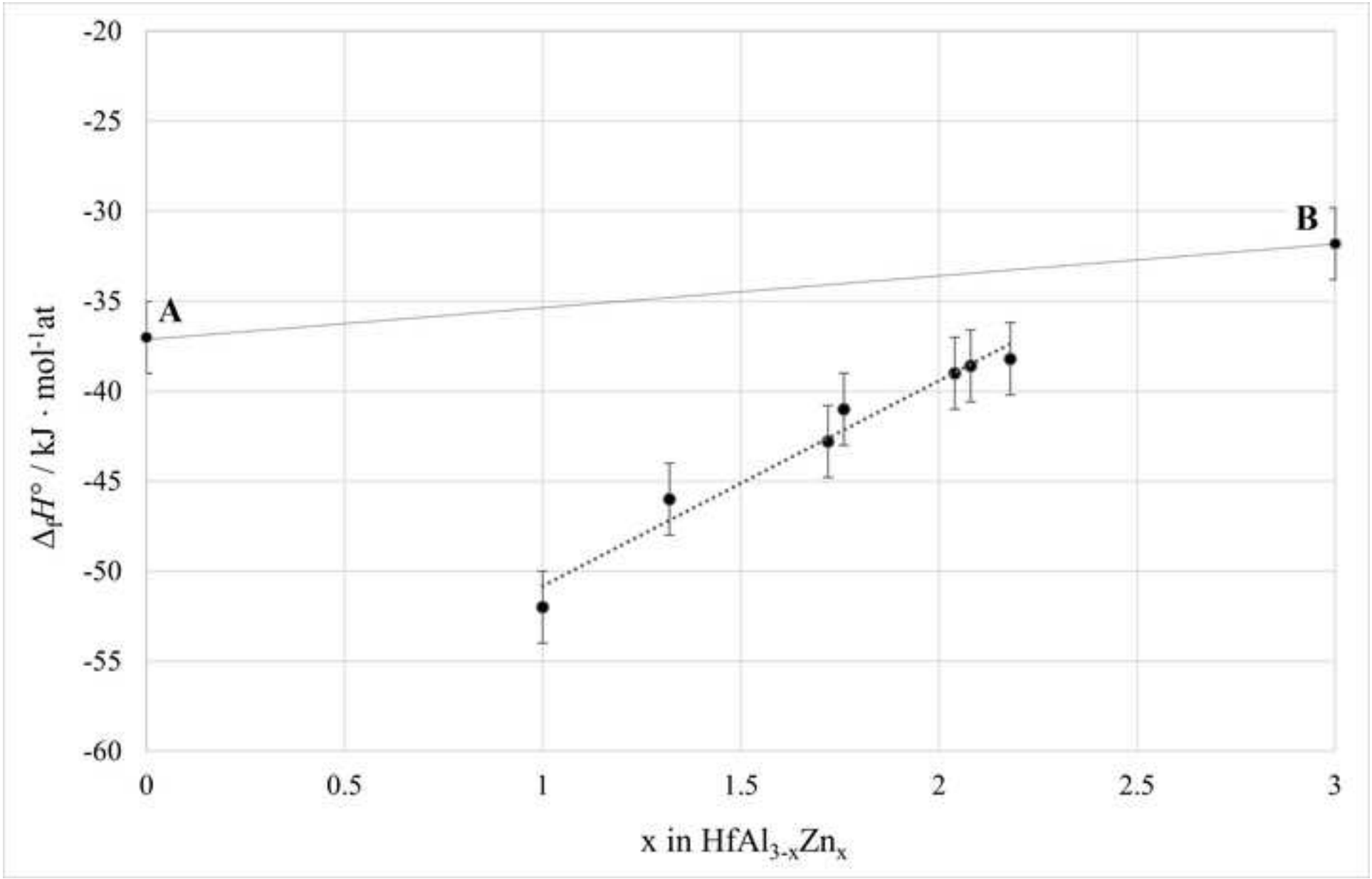

Figure

Click here to access/download;Figure;Figure_3_Delsante_Manuscript.tif

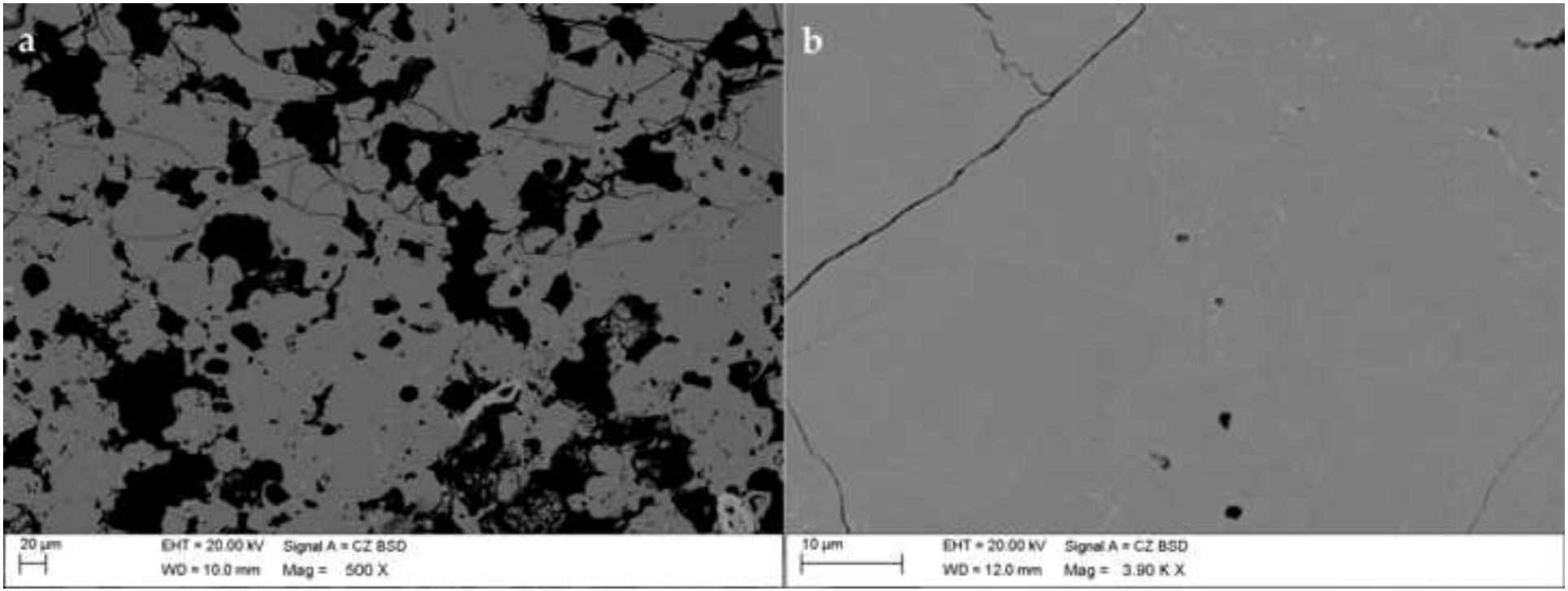

Figure

Click here to access/download;Figure;Figure_4_Delsante_Manuscript.tif

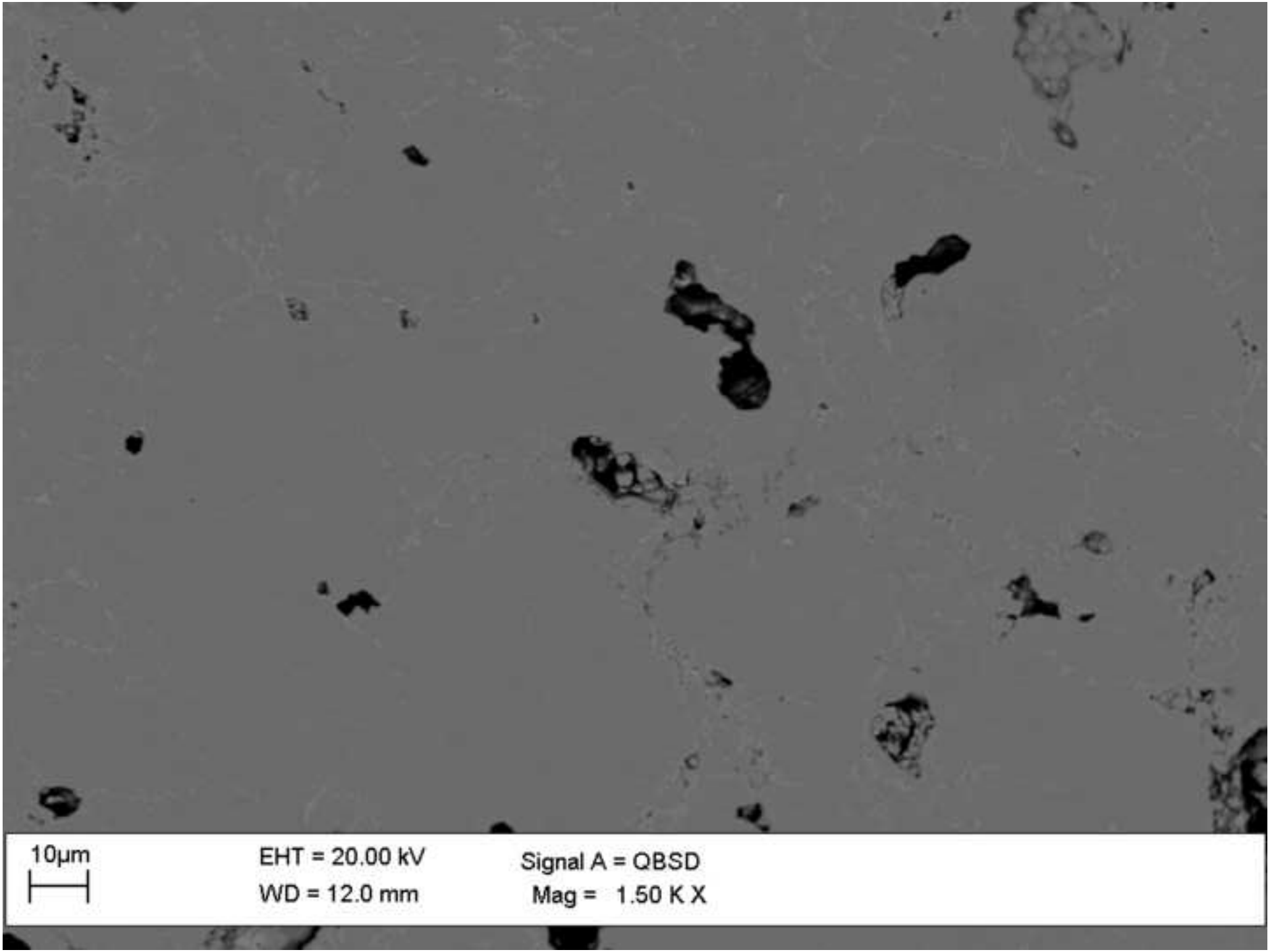

Figure

Click here to access/download;Figure;Figure_5_Delsante_Manuscript.jpg

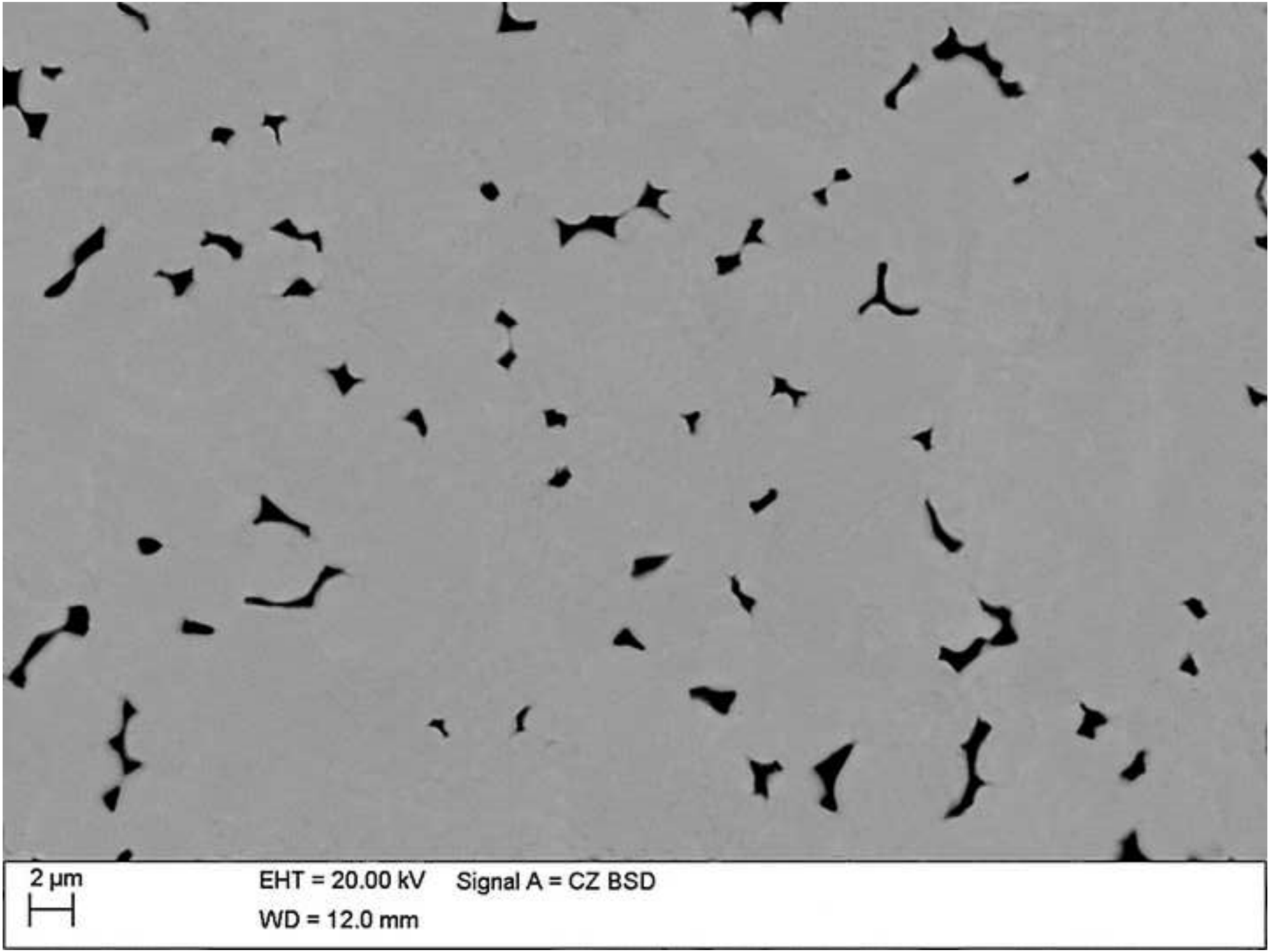

Figure

Click here to access/download;Figure;Figure_6_Delsante_Manuscript_Revised.jpg

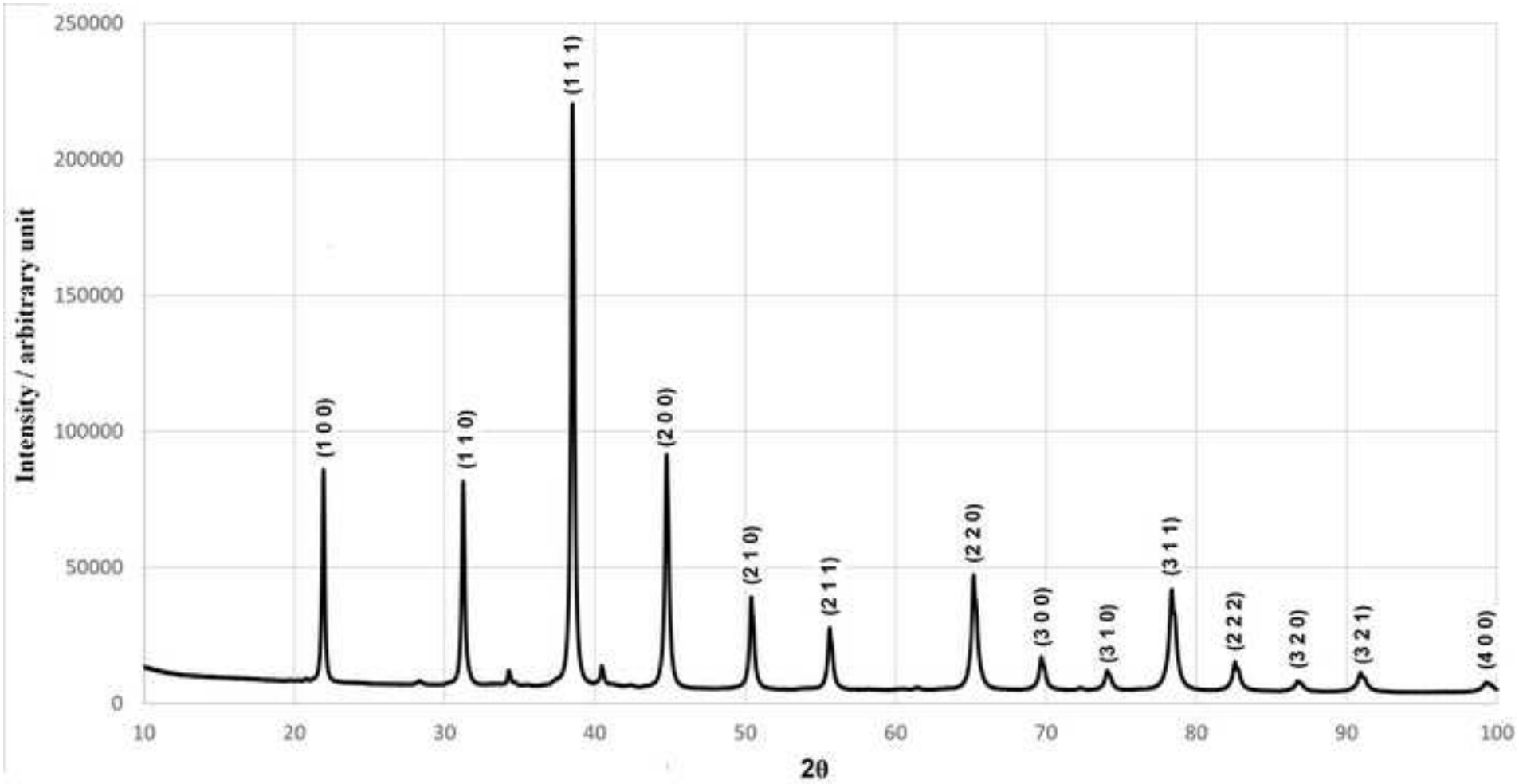

Figure

Click here to access/download;Figure;Figure_7_Delsante_Manuscript.jpg

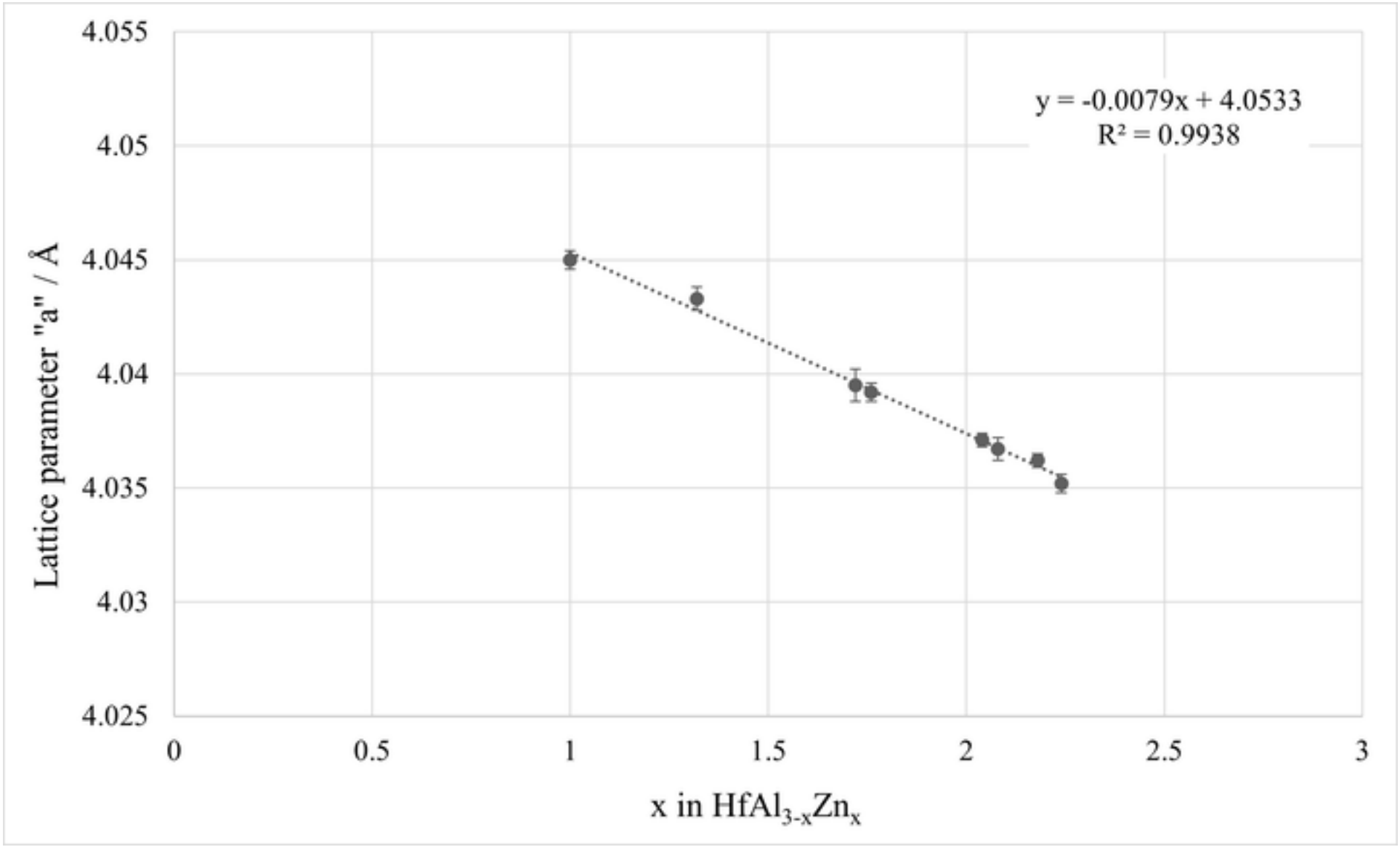

Table 1: Data selection of the synthesized calorimetric binary and ternary samples. The following information have been inserted: global EDS composition, calorimeter working temperature (T_c), $\Delta_f H°$ at 300K obtained by H.T. drop calorimetry, observed phases by SEM/EDS and XRPD analysis, lattice parameter of the $HfAl_{3-x}Zn_x$ cubic phase ($L1_2$). The following values of $\Delta_f H°$ (kJ/mol-atom at) of $L1_2$–$HfAl_{3-x}Zn_x$ are obtained by interpolation of our experimental data: -37.1±2.0 ($HfAl_{0.8}Zn_{2.2}$ corresponding to $Hf_{25}Al_{20}Zn_{55}$ at. %), -41.7±2.0 ($HfAl_{1.2}Zn_{1.8}$ corresponding to $Hf_{25}Al_{30.0}Zn_{45.0}$ at. %), -45.1±2.0 ($HfAl_{1.5}Zn_{1.5}$ corresponding to $Hf_{25}Al_{37.5}Zn_{37.5}$ at. %) and -48.5±2.0 ($HfAl_{1.8}Zn_{1.2}$ corresponding to $Hf_{25}Al_{45.0}Zn_{30.0}$ at. %).

#	Global EDS composition (at. %)			T_c / K (±2)	$\Delta_f H°$ kJ/mol-atom	Observed phases by XRPD and SEM/EDS analyses & comments	Lattice parameters (Å) of cubic $HfAl_{3-x}Zn_x$ phase (x value in brackets)
	Hf	Al	Zn				
1	24.5	75.5	-	1089	-37.0±2.0	Nearly one-phase sample of $HfAl_3$. Small quantity of $HfAl_2$. See text for lattice parameters determination.	
2	24.0	-	76.0	1085	-31.8±3.0	~85% of $HfZn_3$ phase and ~15% of a phase having a composition ~ $Hf_{22}Zn_{78}$ *See figure 1*	
3	25.0	15.0	60.0	1067	-35.5±2.0	Two-phase sample: cubic phase $HfAl_{3-x}Zn_x$ (x = 2.24, ~$Hf_{25.0}Al_{19.0}Zn_{56.0}$ at. %) and a phase having a composition ~$Hf_{25.0}Al_{9.0}Zn_{66.0}$ at. %	a = 4.0352(4) (x = 2.24)

4	25.5	21.0	53.5	1070	-38.2±2.0	Almost single cubic phase $HfAl_{3-x}Zn_x$ (x = 2.18, ~$Hf_{25.0}Al_{20.5}Zn_{54.5}$ at. %). *See figure 3*	*a* = 4.0362(3) (x = 2.18)
5	26.5	25.0	48.5	1067	-38.6±2.0	More than 95% of $HfAl_{3-x}Zn_x$ cubic phase (x = 2.08, ~$Hf_{25.0}Al_{23.0}Zn_{52.0}$ at. %).	*a* = 4.0367(5) (x = 2.08)
6	26.0	23.0	51.0	1070	-39.0±2.0	More than 95% $HfAl_{3-x}Zn_x$ cubic phase (x = 2.04, ~$Hf_{25.0}Al_{24.0}Zn_{51.0}$ at. %). *See figure 4*	*a* = 4.0371(3) (x = 2.04)
7	24.5	31.5	44.0	1068	-41.0±2.0	More than 95% $HfAl_{3-x}Zn_x$ cubic phase (x = 1.76, ~$Hf_{25.0}Al_{31.0}Zn_{44.0}$ at. %). *See figure 6*	*a* = 4.0392(4) (x = 1.76)
8	25.5	31.5	43.0	1065	-42.8±2.0	More than 95% $HfAl_{3-x}Zn_x$ cubic phase (x = 1.72, ~$Hf_{25.0}Al_{32.0}Zn_{43.0}$ at. %).	*a* = 4.0395(7) (x = 1.72)
9	25.5	42.5	32.0	1068	-46.0±2.0	More than 95% $HfAl_{3-x}Zn_x$ cubic phase (x = 1.32, ~$Hf_{25.0}Al_{42.0}Zn_{33.0}$ at. %). *See figure 5*	*a* = 4.0433(5) (x = 1.32)
10	25.0	47.0	28.0	1073	-52.0±2.0	Nearly single $HfAl_{3-x}Zn_x$ cubic phase (x = 1.0, ~$Hf_{25.0}Al_{50.0}Zn_{25.0}$ at. %).	*a* = 4.0450(4) (x = 1.0)

Università di Genova | DCCI
Dipartimento di Chimica e Chimica Industriale

Genoa,1-08-2024

I can confirm with the other authors that there is no conflict of interest, including any financial, personal, or other relationships with other people or organizations that could inappropriately influence, or be perceived to influence, our work.

Truly,

Simona Delsante.

Prof. Simona Delsante, PhD
Università degli Studi di Genova
Dipartimento di Chimica e Chimica Industriale
Via Dodecaneso 31, 16146 Genova, Italy
Tel.+39 0103536160/Fax +39 0103625051
e-mail: simona.delsante@unige.it

Author Statement*

In the following are reported the roles of each author involved in the submitted work "Experimental determination of phase stability of the cubic $L1_2$ $HfAl_{3-x}Zn_x$ phase" by S. Delsante, G. Borzone, N. Parodi and S. Guerrucci, to be published in the "*Thermochimica Acta*" Journal.

Simona Delsante (Professor):

Conceptualization, Formal analysis, Supervision, Writing – original draft and Writing – review & editing

Gabriella Borzone (Retired Professor):

Conceptualization and Supervision

Nadia Parodi (Researcher):

Data curation and Visualization

Sara Guerrucci (PhD student):

Investigation and Methodology

Experimental determination of phase stability of the cubic $L1_2$ $HfAl_{3-x}Zn_x$ phase

S. Delsante[a,b*], G. Borzone[a,b], N. Parodi[a], S. Guerrucci[a]

[a]*Department of Chemistry and Industrial Chemistry, Genoa University, Via Dodecaneso 31 – I-16146 Genoa – Italy and Genoa Research Unit of the National Consortium of Materials Science and Technology (INSTM) – ITALY*

[b]*Institute of Condensed Matter Chemistry and Technologies for Energy, National Research Council of Italy (ICMATE-CNR), Via De Marini 6, 16149 Genoa, Italy*

[*]Corresponding Author: simona.delsante@unige.it

Abstract

The present study is devoted to the experimental investigation of homogeneity range and heat of formation ($\Delta_f H°$ at 300K) of the cubic $L1_2$–$HfAl_{3-x}Zn_x$ solid solution. A high-temperature direct drop calorimeter has been employed to synthesize and simultaneously determine the $\Delta_f H°$ of several alloys along the $HfZn_3$–$HfAl_3$ section (25 at. % Hf) whereas X-Ray Powder Diffraction (XRPD) and Scanning Electron Microscopy (SEM) paired with an EDS (Energy Dispersive Spectrometer detector) have been employed to characterize the samples. The performed analysis confirmed that the ternary $HfAl_{3-x}Zn_x$ alloys were nearly single phase in the range $1 \leq x \leq 2.24$ having the cubic $L1_2$ structure; this in turn helps establish the trend of $L1_2$ lattice parameter (at room temperature) with composition. Thanks to the interpolation of our experimental data, the following values of $\Delta_f H°$ (kJ/mol-atom at 300K) for the $L1_2$–$HfAl_{3-x}Zn_x$ were determined: -37.1±2.0 ($HfAl_{0.8}Zn_{2.2}$ corresponding to $Hf_{25}Al_{20}Zn_{55}$ at. %), -41.7±2.0 ($HfAl_{1.2}Zn_{1.8}$ corresponding to $Hf_{25}Al_{30.0}Zn_{45.0}$ at. %), -45.1±2.0 ($HfAl_{1.5}Zn_{1.5}$ corresponding to $Hf_{25}Al_{37.5}Zn_{37.5}$ at. %) and -48.5±2.0 ($HfAl_{1.8}Zn_{1.2}$ corresponding to $Hf_{25}Al_{45.0}Zn_{30.0}$ at. %). For two pertinent binary intermetallic phases, the following $\Delta_f H°$ values (in kJ/mol-atom) at 300K have been obtained: -31.8±3.0 for $HfZn_3$ (unknown structure) and -37.0±2.0 for $HfAl_3$ (tetragonal DO_{23} – type structure).

Keywords*: Trialuminides; Thermodynamic and thermochemical properties; Calorimetry; X-Ray Powder Diffraction.*

Highlights

- $\Delta_f H°$ at 300 K of several $HfAl_{3-x}Zn_x$ alloys have been measured by H.T. calorimetry
- Calorimetric data have been validated by XRPD and SEM-EDS analysis
- The trend of $\Delta_f H°$ *vs.* x for the cubic $L1_2$ - $HfAl_{3-x}Zn_x$ phase has been obtained
- The range of existence of the cubic $L1_2$ - $HfAl_{3-x}Zn_x$ phase has been determined

1. Introduction

Intermetallic compounds have long fascinated scientists from different fields due to their peculiar and often unpredictable crystal structures [1–6], chemical bonding [7–11], and both physical [12–16] and mechanical properties [17].

Among them, trialuminides with cubic structure ($L1_2$ or $cP4$–$AuCu_3$ type) have long been considered as ductile, low density structural materials for high-temperature applications and to exploit the possibility of using them as precipitates to improve the creep resistance of aluminium-based alloys at high temperatures. However, many trialuminides crystallise with a tetragonal structure (DO_{22}–$TiAl_3$ or DO_{23}–$ZrAl_3$) that confers an inherent fragility that limits their use in engineering applications [18-21].

These premises stimulated the research for alloying elements that would stabilise the cubic structure for the $TMAl_3$ (*TM* = transition metal) phase at the expense of the tetragonal one. Among relevant binary alloy systems, dilute Al–Sc alloys are heat treatable; solid-state aging leads to nanoscale precipitation of coherent $L1_2$–$ScAl_3$ as an equilibrium phase in an (Al) matrix and such a microstructure exhibits significant creep resistance for the Al alloys [22, 23]. Although, the high cost of Sc could be a prohibitive factor. The cubic $L1_2$–$REAl_3$ compounds as equilibrium phases is present in several Al–rare earth systems (*RE* = Er, Tm, Yb, Lu); however, these Al–*RE* alloys are not easily heat-treatable due to the small solubility towards Al of these RE elements [24].

The ternary cubic $L1_2$ phases based on $TiAl_3$ phase are reported for a certain number of Al–Ti–*X* (*X* = V, Cr, Mn, Fe, Co, Ni, Cu, Zn, Nb, Mo, Rh, Pd, Ag, Pt, and Au) systems [25]; however, an equilibrium tie-line between (Al) and the cubic $L1_2$ phase has not been observed in available experimental ternary phase diagrams. This is due to the presence of phase equilibria concerning Al–Ti and Al–X intermetallic phases and ternary compounds.

Based on these considerations, it is worth seeking ternary alloy compositions that allow the formation of a microstructure with nanometric precipitates of a thermodynamically stable $L1_2$ cubic phase not containing any expensive alloying element to design Al alloys for high-temperature applications. We have already investigated the stability of $TiAl_{3-x}Zn_x$ alloys to probe the possibility of introducing thermodynamically stable $L1_2$–$TMAl_{3-x}Zn_x$ precipitates in an (Al) matrix [26]; this was prompted by the

hereafter factors: (i) Al–Zn system do not shows the presence of any intermetallic phases, (ii) the equilibrium $L1_2$–$TiZn_3$ phase can dissolve a substantial amount of Al [27] and (iii) the total energy and electronic structure calculations of $TiAl_{3-x}Zn_x$ alloys using first-principles methods show that in these systems it is possible to stabilize $L1_2$ structure while destabilizing DO_{22} and DO_{23} structures [28, 29]. Formation of metastable $L1_2$–$HfAl_3$ is well documented in the literature but the $L1_2$ phase undergoes transformation to the equilibrium DO_{23}–$HfAl_3$. For example, metastable $L1_2$–$HfAl_3$ forms in an Al-matrix during solid state aging of dilute Hf–Al alloys [30] and Srinivasan *et al.* reported that the mechanically alloyed $L1_2$–$HfAl_3$ transforms directly to DO_{23}–$HfAl_3$ at about 1023 K [31]. Nevertheless, the existence of ternary $TMAl_{3-x}Zn_x$ $L1_2$ phases was reported for Zr–Zn–Al and Hf–Zn–Al systems [27, 32].

Here, we present the results of thermodynamic and structural properties investigation of $HfAl_{3-x}Zn_x$ alloys synthesized by direct reaction calorimetry, and subsequently characterized by several well-concerted techniques.

2. Literature review

Literature data about the two binary boundary systems relevant to this investigation are discussed below.

The studies on the Hf–Al phase diagram date back to 1998 by Murray et al. [33] and one of the accepted versions is reported in [34] where the phase diagram was calculated using CALPHAD (CALculation of PHAse Diagram) method. In the Al-rich part (> 30 at. %), there are three intermetallic compounds: Hf_2Al_3, $HfAl_2$ and $HfAl_3$ which melt congruently; nevertheless, the liquidus curves are traced as dotted lines demonstrating the low reliability of this part of the diagram. As for the $HfAl_3$ phase, two polymorphs are considered [33, 34]: one stable below 923 K ($\alpha HfAl_3$, DO_{22} or $tI8$–Al_3Ti) and one stable at higher temperature ($\beta HfAl_3$, DO_{23} or $tI16$–Al_3Zr) which melts congruently around 1863 K.

However, a further consideration of published literature shows that the temperature range of stability of $HfAl_3$ is controversial. Schübert et al [60Sch] reported that $\alpha HfAl_3$ is stable only in the temperature range 973 ÷ 1223 K, and several others reported that $\beta HfAl_3$ is the low temperature form [36-39]. Pötzschke and Schübert [37]

reported the persistence βHfAl$_3$ after prolonged heat treatment of αHfAl$_3$ at 723 K while in [31] it has been reported that the mechanically alloyed *L*1$_2$–HfAl$_3$ transforms directly to *DO*$_{23}$–HfAl$_3$ at about 1023 K. Due to these conflicting data, the latest assessment of Hf–Al phase equilibria [40] shows only βHfAl$_3$, *DO*$_{23}$ (t*I*16–Al$_3$Zr), as the equilibrium phase.

Available calorimetric data of Hf–Al intermetallics [41, 42] have been reviewed elsewhere [34, 43, 44]. Meschel and Kleppa [41] employed direct reaction calorimetry at 1473 K, and reported formation enthalpies of HfAl$_3$, HfAl$_2$ and HfAl. Balducci *et al.* [42] measured vapour pressure of aluminium in the 50–75 at. % Al composition range using Knudsen cell-mass spectrometry in the temperature range 1280 ÷ 1680 K. The enthalpy changes of the decomposition reactions were calculated by the "second-law" and "third-law methods".

The phase diagram of the Hf–Zn system is not known [24]. The following intermetallics have been identified: HfZn$_2$, HfZn$_3$, HfZn$_5$ and HfZn$_{22}$; among these, HfZn$_3$ is reported to exhibit two allotropic forms: a high-temperature form with an unidentified complex structure and a room-temperature form with a tetragonal structure *t***–ZrZn$_3$ whose details have not yet been solved [45]. No thermodynamic experimental data are available; nonetheless, first-principles calculations [28] shows that, among the three structures considered (*DO*$_{22,}$ *DO*$_{23}$ and *L*1$_2$), the cubic one is found to have the lowest energy for HfZn$_3$.

There is no report of phase diagram and thermochemistry of Hf–Zn–Al alloys; only the crystal structure data of few ternary alloys has been reported by Raman and Schübert [27], Schübert *et al.* [32] and Drasner and Blazina [46]. At 973 K, Schubert and co-workers [27, 32] obtained single-phase alloys, in the composition range of HfAl$_{3-x}$Zn$_x$ ($1 \leq x \leq 2.2$) having *L*1$_2$ (*cP*4–AuCu$_3$) type structure. On the other hand, Drasner and Blazina [46] found a single-phase region HfAl$_{2-x}$Zn$_x$ ($0.5 \leq x \leq 1.25$) in samples annealed at 1273 K for 192h having a cubic structure isotypic with *cF*24–type Laves phase.

3. Experimental

3.1. High-temperature drop calorimetry

Pellets for the synthesis of the samples were prepared with powders of the pure

elements (Al: 99.95%, -325 mesh; Hf: 99.6%, -325 mesh; Zn: 99.999%, -200 mesh; *Alfa Aesar*, Ward Hill, MA).

Adequate amounts of Al, Hf and Zn powders, for several $HfAl_{3-x}Zn_x$ ($0.8 \leq x \leq 2.4$) compositions of alloys were weighed (typically 0.8 ÷ 1.0 g) and mixed in a glove box; in addition, several binary samples having a composition corresponding to the $HfZn_3$ and $HfAl_3$ stoichiometry have been prepared. After powders mixing and pressing, the obtained pellets were enclosed in a tight-sealed tantalum crucible: the preparation of the calorimetric samples starting from a mixture of fine powders and the adopted procedure (see description in the following) secures a fast reaction between different metals, thus minimizes zinc loss due to evaporation. Indeed, no significant zinc loss was detected in the post-calorimetry by SEM/EDS analyses.

Samples have been synthetized inside a high temperature calorimeter in order to measure directly the heat of formation of the alloys; a laboratory built high–temperature (H.T.) drop calorimeter was employed, whose detailed description is given elsewhere [47, 48]. Each measurement is divided into two series: a "*reaction run*" and a "*reference run*", as described in various previous publications [49-52]. During the "*reaction run*", after thermal equilibration, the sample is dropped from an above thermostat (at $T = T_0 = 300$ K) into the calorimetric cell maintained at a chosen T_c (during this work around 1073K, see table 1). The heat effect is calculated by exploiting the calibration procedure: it consists of a series of "*calibration runs*" carried out by dropping samples of known heat content (typically pieces of pure Ag weighing 0.8 ÷ 1.2g) in the same condition.

The reactions occurring for ternary samples and the equations allowing to determine the measured heat are shown below. The same equations can be applied to binary samples.

In the "*reaction run*" the heat effect Q_1 is due to the solid-state reaction (*"cr"* stands for *"crystalline"*):

$$x\mathrm{Hf}(cr,T_c) + y\mathrm{Al}(cr, T_c) + z\mathrm{Zn}(cr, T_c) \rightarrow \mathrm{Hf_xAl_yZn_z}\ (cr, T_c) \qquad \text{at temperature } T_c \qquad (1)$$

and to the increment of enthalpy of Al, Hf, Zn and of the tantalum crucible (*cruc*).

Hence, Q_1 for 1 mol of alloy $Hf_xAl_yZn_z$ can be expressed as:

$$Q_1 = x\,(H_{Tc} - H_{T0})(\mathrm{Hf},cr) + y\,(H_{Tc} - H_{T0})(\mathrm{Al},cr) + z\,(H_{Tc} - H_{T0})(\mathrm{Zn},cr) + m_{cruc}\,(H_{Tc} - H_{T0})(\mathrm{Ta}, cruc) + \Delta_f H(\mathrm{Hf_xAl_yZn_z}, cr, T_c) \qquad (2)$$

In the "*reference run*", the heat effect Q_2 is due to the enthalpy increments of the alloy and of the tantalum crucible, and is written as:

$$Q_2 = (H_{Tc} - H_{T0})(Hf_xAl_yZn_z, cr) + m_{cruc}(H_{Tc} - H_{T0})(Ta, cruc) \quad (3)$$

Considering the difference ($Q_1 - Q_2$), the effects of the crucible cancel out and it is possible to obtain the $\Delta_f H(Hf_xAl_yZn_z, cr, T_c)$, corrected for the difference in the heat contents of metals and alloy, that is the $\Delta_f H(Hf_xAl_yZn_z, cr, T_0)$ at T_0.

$$Q_1 - Q_2 = \Delta_f H\,(Hf_xAl_yZn_z, cr, T_0) \quad (4)$$

The standard uncertainty in $\Delta_f H\,(Hf_xAl_yZn_z, cr, T_0)$, is higher when its value is small compared to Q_1 and Q_2. Since Q_1 and Q_2 increase proportionally with temperature and $\Delta_f H$ is generally nearly temperature independent, the lowest temperature that allows a complete reaction is generally chosen. The errors associated to the measurement are estimated to be ±0.3 to 0.5 kJ/mol-atom in any run, and the accuracy of calorimetric results is linked to the actual processes taking place in the calorimeter. The calibration constant of the calorimeter was obtained by dropping several specimens of known heat content as a function of the total mass inside the measuring cell. Furthermore, it has been observed that the sensitivity is independent of the size of heat effect in the energy range 50 ÷ 1000J [47]. For an overall assessment of the error, the following factors should be considered: (i) completeness of the synthesis reaction; (ii) achievement of the equilibrium state; (iii) presence/absence of side reactions, etc.

The composition of the samples and the working temperature of the calorimetric cell were selected on the basis of available information and our previous experience on Al–Ti–Zn system [26], to have fast synthesis reactions. After the calorimetric experiments, microscopic analysis (Light Optical Microscopy – LOM and Scanning Electron Microscopy coupled with electron probe microanalysis – SEM/EDS) and X-Ray Powder Diffraction Analysis (XRPD) were used to check the composition and state of the samples.

3.2. X-Ray Powder Diffraction

X-Ray Powder Diffraction (XRPD) was performed after crushing the samples in a agate mortar using a Philips *X'Pert MPD* machine (Philips, Almeno, The Netherlands) equipped with a copper target, excited to 40 kV and 30 mA, and a solid-state detector. The XRPD patterns were indexed by *PowderCell* [53] and the lattice parameters were obtained by a least-squares routine [54]; this procedure allows to identify the formed phases and experimentally measure the lattice parameters.

It is worth pointing out that XRPD results of samples are obtained using directly synthesized samples that were cooled at an estimated rate of 1°C/min from T_c to room temperature.

3.3. Microstructural characterization

Samples for the microstructural characterization have been prepared by grinding, lapping and polishing the resin-mounted pieces of alloys; the final steps to obtain a mirror-like surfaces have been performed using diamond abrasive spray down to 1 μm grain size.

A Light Optical Microscope (LOM) was employed to have an overview of the microstructure (i.e. number and phase distribution); no etching was necessary to recognize the phases. Then, each sample was investigated with a Scanning Electron Microscope (SEM, Zeiss EVO 40*"Carl Zeiss SMT Ltd*., *Cambridge, England"* operating at 20 kV); a Back Scattered Electron detector (BSE) was employed to reveal the compositional contrast between the different phases whilst an Energy Dispersive Spectrometer (EDS, Oxford INCA *X-ACT*) detector was exploited to collect quantitative data both on global and phase composition. The package Inca Energy (Oxford Instruments, Analytical Ltd., Bucks, U.K.) software was employed to process the EDS spectra; generally, an error within 0.5 at. % was assigned for each element.

4. Results and discussion

The samples synthesis takes place during the calorimetric experiments, so it is possible to directly measure the enthalpy of formation of the alloys; because of this, is pivotal to check the equilibrium state reached by the sample to obtain reliable $\Delta_f H°$ results. To this end, the vol. % of the formed phases together with their composition were

estimated/determined by LOM, SEM/EDS and XRPD analysis. For examples, in some cases unreacted Hf was found, which probably leads to an underestimation of the alloy's $\Delta_f H°$ and, consequently, the rejection of the calorimetric result.

A summary of the reliable binary and ternary prepared samples together with the calorimetric results and the performed characterization is inserted in table 1; in addition, a brief comment on the peculiarities of the samples was included. The temperature of the calorimetric cell (T_c) was set considering several preliminary tests runs and our previous investigations on Ti–Zn [55] and Al–Ti–Zn [26] alloys. Indeed, during this study, we faced the same experimental difficulties previously encountered due to intrinsic factors of the system such as a large difference in melting points between Hf, Al and Zn and high vapour pressure of Zn.

A detailed discussion of the results obtained can be found in the following sections.

4.1. $HfAl_3$ and $HfZn_3$ phases

We obtained $\Delta_f H°$ (300K) = -37.0±2.0 kJ/mol-atom for the $HfAl_3$ phase: this value is in good agreement with the one reported by Meschel and Kleppa [41] (-40.6±0.8 kJ/mol-atom) but shows an expectedly large disagreement with the value (-44.7±2.4 kJ/mol-atom) reported by Balducci *et al.* [42]. It should be noted that Meschel and Kleppa [41] performed direct reaction calorimetry at 1473K while Balducci *et al.* [42] carried out vapor pressure measurements in the temperature range of 1280 ÷ 1680 K. Unfortunately, these authors did not report the observed structure of $HfAl_3$. Our experimental value of $\Delta_f H°$ is consistent with the formation energy of DO_{23}–$HfAl_3$, -37.3 [43], -38.65 [44] kJ/mol-atom and -38.69 kJ/mol [56] calculated from first-principles methods.

X-Ray diffraction performed on the sample (#1 in table 1) revealed the presence of the $HfAl_3$ phase having DO_{23} (t*I*16–Al_3Zr) structure which is now believed to be the only stable form of this phase; this is consistent with the latest assessment of Hf–Al phase diagram [40] and with earlier experiments [36-39]. A few additional diffraction peaks were also present and attributed to the $HfAl_2$; this was further confirmed by SEM/EDS analysis. The measured lattice parameters of DO_{23}–$HfAl_3$ (a = 3.988(4) Å, c = 17.14(2) Å) are in good agreement with those reported in literature (a = 3.982 Å and c = 17.139 Å [35]; a = 3.982 Å and c = 17.15 Å [36]; a = 3.919 Å and c = 17.653 Å [38]; a = 3.987 Å

and c = 17.15 Å [39]).

After several attempts, we obtained a value of $\Delta_f H°$ (at 300K) = -31.8±3.0 kJ/mol-atom for a sample containing the $HfZn_3$ as majority phase (~85%) (#2 in table 1). A typical SEM micrograph (BSE mode) of this "*as-synthesized*" alloy is shown in figure 1: the bright phase corresponds to the ~$Hf_{25}Zn_{75}$ at. % ($HfZn_3$ stoichiometry) and the dark grey one has a composition ~ $Hf_{22}Zn_{78}$ at. %. The latter may be related to a coring effect [57] occurred during the cooling, and possibly due to sluggish reaction in the solid state as well as the formation of transient phase(s). The crystal structure of this phase is not known [24]; even though we have performed XRPD, a detailed analysis to obtain lattice parameters could not be performed.

4.2 $HfAl_{3-x}Zn_x$ phase

The composition dependence of $\Delta_f H°$ for the $HfAl_{3-x}Zn_x$ cubic $L1_2$ phase is shown in figure 2 based on the calorimetric results reported in table 1; in this study, an error associated with the measurement of $\Delta_f H°$ is estimated to generally be ±2.0 (kJ/mol-atom). The trend of the enthalpy of formation shows an increase of the exothermicity for the formation of this phase with the increase of the Al content. The $\Delta_f H°$ value related to sample #3 is not inserted in the trend due to the presence of two phases: the cubic $L1_2$–$HfAl_{3-x}Zn_x$ (x = 2.24, corresponding to an Al content of 19 at. %, which is therefore considered the stability limit of the $L1_2$ phase) together with a phase having a composition ~$Al_9Hf_{25}Zn_{66}$ (at. %). This observation by SEM/EDS is confirmed by the diffraction pattern in which some few additional peaks are present together with the peaks belonging to the cubic phase.

Figure 2 also shows the trend of $\Delta_f H°$ in a limiting case: the line *AB* defines the $\Delta_f H°$ if we assume the ternary alloys along the $HfAl_3$–$HfZn_3$ section to be an ideal mechanical mixture of $HfZn_3$ (unknown structure) and DO_{23}–$HfAl_3$ determined in this work. Our calorimetry data clearly exhibit a strong negative deviation from the ideal behaviour demonstrating that the enhanced stability of ternary alloys is due to both alloying and the formation of the cubic $L1_2$ structure. This general behaviour was also observed by Ghosh et al. [28] even though the experimental enthalpy values for the cubic phase determined in this work are more exothermic than those calculated.

Figure 3 shows the microstructure aspect at two magnifications (500X and 3900X) of the sample (#4 in table 1): the specimen is almost single-phase with the presence of some cracks and holes due to the brittleness of the alloy mainly due to the sample synthesis method (3a, lower magnification); at higher magnification (3b) the presence of a predominant phase is clear. The same feature can be observed in figures 4 and 5 which refers to sample #6 and (#9) in table 1, respectively: the SEM/BSE images show the presence of a predominant phase and some porosities.

The X-ray diffraction analysis of the calorimetrically synthesized specimens from #4 to #10, confirmed that they are almost single-phase samples containing the cubic $L1_2$ phase (c*P*4–$AuCu_3$). As example, figure 6 shows the indexed XRPD pattern of sample #7 in table 1) in which all major peaks are attributed to cubic $L1_2$ structure.

The composition dependence of lattice parameter *"a"* of $L1_2$–$HfAl_{3-x}Zn_x$ is shown in Figure 7 (by using the data reported in table 1): an increase of *"a"* with Al-content may be noticed; this is consistent with the expected behaviour, as the atomic size of Al is larger than Zn. Extrapolation of present data gives the lattice parameter for the $L1_2$–metastable phases as a = 4.0296 Å for $HfZn_3$, and a = 4.0533 Å for $HfAl_3$. The experimental lattice parameter of $L1_2$–$HfAl_3$ obtained by ball-milling [31] is reported to be 4.0480 Å, while first-principles calculations give 4.0807Å [44]; therefore, present results are in fairly good agreement with both experimental and first-principles data.

Figure 7 provides important information regarding the design of new Al-based alloys containing fully coherent and coarsening resistant cubic $L1_2$ precipitates, where it is desirable to design alloys with near-zero misfit strain: $HfAl_{3-x}Zn_x$–based $L1_2$ phase may satisfy this criterion because they will not cause a significant lattice mismatch with Al (a = 4.0496 Å).

5. Conclusions

As a part of our study of phase stability of ternary alloys with $L1_2$ structure, direct reaction calorimetry has been carried out using a high-temperature drop calorimeter on ternary alloys having a composition $HfAl_{3-x}Zn_x$ ($0.8 \leq x \leq 2.4$) which are located along the section $HfAl_3$–$HfZn_3$. In addition, the same measurements were performed on the binary samples with $Hf_{25}Al_{75}$ and $Hf_{25}Zn_{75}$ at. % content.

The presence of the desired phase, its atomic compositions and lattice parameters were determined by SEM/EDS and XRPD measurements to define the reliability of the calorimetric data.

Interpolation of the $\Delta_f H°$ experimental values for $L1_2$–$HfAl_{3-x}Zn_x$ solid solution allows us to estimate the heat of formation at 300K for several discrete compositions such as -37.1±2.0 ($HfAl_{0.8}Zn_{2.2}$ corresponding to $Hf_{25}Al_{20}Zn_{55}$ at. %), -41.7±2.0 ($HfAl_{1.2}Zn_{1.8}$ corresponding to $Hf_{25}Al_{30.0}Zn_{45.0}$ at. %), -45.1±2.0 ($HfAl_{1.5}Zn_{1.5}$ corresponding to $Hf_{25}Al_{37.5}Zn_{37.5}$ at. %) and -48.5±2.0 ($HfAl_{1.8}Zn_{1.2}$ corresponding to $Hf_{25}Al_{45.0}Zn_{30.0}$ at. %). An increase of exothermicity is observed for the $HfAl_{3-x}Zn_x$ alloys with the increasing of the Al content, confirming the stabilization of $L1_2$–$HfAl_{3-x}Zn_x$ phase by substituting Zn with Al.

The measured Al composition for the cubic phase ($L1_2$) ranges from $Hf_{25}Al_{50}Zn_{25}$ to $Hf_{25}Al_{19}Zn_{56}$ at. % (corresponding to $1 \leq x \leq 2.25$ in $HfAl_{3-x}Zn_x$) and is in good agreement with data reported by Schubert and coworkers [27, 32].

Implications of our results have been briefly discussed in the context of design of aluminium based alloys containing thermodynamically stable and coherent $L1_2$ phase. Our experimental thermodynamic data can be compared with the values obtained using the "*Open Quantum Materials Database (OQMD)*" [58] and the calculated heats of formation of $L1_2$, DO_{22}, DO_{23} phases along the pseudo-binary section Al_3Hf–Zn_3Hf. Even the increasingly exothermic nature of the formation enthalpy of the investigated ternary phases with increasing Al content is also confirmed in both references, the experimental values are more exothermic than the calculated ones. In addition, values calculated in [58] would not seem to confirm the presence of a continuous cubic $L1_2$ solid solution in the considered range whereas in [28] the $L1_2$ cubic phase seems to be the more stable. For this reason, this work is also an excellent incentive for further ab initio studies on the stability of the cubic ternary phase compared to those with a tetragonal structure, in order to understand this discrepancy and expand knowledge on this interesting class of materials.

References

[1] W. Steurer, J. Dshemuchadse, Crystal structures of intermetallic compounds, Intermetallics: Structures, Properties, and Statistics (2016) Oxford Academic.

[2] A.P. Tsai, J.Q. Guo, E. Abe, H. Takakura, T.J. Sato, A stable binary quasicrystal, Nature, 408 (2000) 537–538.

[3] Y. Grin, Crystal Structure and Bonding in Intermetallic Compounds, Comprehensive Inorganic Chemistry II, (2013) Elsevier, 359–373.

[4] L. Agnarelli, Y. Prots, R. Ramlau, M. Schmidt, U. Burkhardt, A. Leithe-Jasper, Y. Grin, $Mg_{29-x}Pt_{4+y}$: Chemical Bonding Inhomogeneity and Structural Complexity, Inorg. Chem., 61, issue 40 (2022) 16148–16155.

[5] O. A. Blatova, M. A. Solodovnikova, E. M. Egorova, V. A. Blatov, Stability of intermetallic compounds: Geometrical and topological aspects, Intermetallics, 164 (2024) 108124.

[6] R. Freccero, S.H. Choi, P. Solokha, S. De Negri, T. Takeuchi, S. Hirai, P. Mele, A. Saccone, Synthesis, crystal structure and physical properties of $Yb_2Pd_3Ge_5$, J. Alloys Compd. 783 (2019) 601–607.

[7] R. Nelson, C. Ertural, P. C. Müller, R. Dronskowski, Chemical bonding with plane waves, Comprehensive Inorganic Chemistry III, (2023) Elsevier, 141–201.

[8] F.R. Wagner, Y. Grin, Chemical bonding analysis in position space, Comprehensive Inorganic Chemistry III, (2023) Elsevier, 222–237.

[9] R. Freccero, Y. Grin, F.R. Wagner, Polarity-extended $8 - N^{eff}$ rule for semiconducting main-group compounds with the TiNiSi-type of crystal structure, Dalton Trans. 52 (2023) 8222–8236.

[10] Q. Lin, G.J. Miller, Electron-Poor Polar Intermetallics: Complex Structures, Novel Clusters, and Intriguing Bonding with Pronounced Electron Delocalization, Acc. Chem. Res. 51, issue 1 (2018) 49–58.

[11] A. Lim, D.C. Fredrickson, Navigating the 18-n+m Isomers of $PdSn_2$: Chemical Pressure Relief through Isolobal Bonds and Main Group Clustering, Inorg. Chem. 63, issue 25 (2024) 11726–11736.

[12] X. Tan, Z. P. Tener, M. Shatruk, Correlating Itinerant Magnetism in RCo_2Pn_2

Pnictides (R = La, Ce, Pr, Nd, Eu, Ca; Pn = P, As) to Their Crystal and Electronic Structures, Acc. Chem. Res. 51, issue 2 (2018) 230–239.

[13] A. Martinelli, D. Ryan, J. Sereni, C. Ritter, A. Leineweber, I. Curlik, R. Freccero, M. Giovannini, Magnetic phase separation in the $EuPdSn_2$ ground state, J. Mater. Chem. C, 11 (2023) 7641–7653.

[14] T. Shang, E. Svanidze, T. Shiroka, Probing the superconducting pairing of the $La_4Be_{33}Pt_{16}$ alloy via muon-spin spectroscopy, J. Phys.: Condens. Matter, 36, issue 10 (2023) 105601.

[15] L. M. Sandratskii, V. M. Silkin, L. Havela, Multiple localized-itinerant dualities in magnetism of $5f$ electron systems: The case of UPt_2Si_2, Phys. Rev. Materials, 8 (2024) 034401.

[16] Z. Sobczak, M. J. Winiarski, W. Xie, R. J. Cava, T. Klimczuk, Superconductivity in the intermetallic compound Zr_5Al_4, EPL 127 (2019) 37005.

[17] A. R. Paul, M. Mukherjee, D. Singh, A Critical Review on the Properties of Intermetallic Compounds and Their Application in the Modern Manufacturing, Cryst. Res. Technol. (2021) 2100159.

[18] R.W. Cahn, Combining metals and sciences: ways of investigating intermetallics, Intermetallics, 6, issues 7–8 (1998) 563–566.

[19] A. H. Cottrell, Ductile aluminium and brittle trialuminides, Mat. Sci. Technol., 7, issue 11 (2013) 981–984.

[20] R.B. Schwarz, P.B. Desch, S. Srinivasan, P. Nash, Synthesis and properties of trialuminides with ultra-fine microstructures, Nanostructured materials, 1, issue 1 (1992) 37–42.

[21] D.G. Morris, M.A. Muñoz-Morris, L.M. Requejo, C. Baudin, Strengthening at high temperatures by precipitates in Fe–Al–Nb alloys, Intermetallics, 14 (2006) 1204–1207

[22] D.N. Seidman, E.A. Marquis, D.C. Dunand, Precipitation strengthening at ambient and elevated temperatures of heat-treatable Al(Sc) alloys, Acta Mater., 50, issue 16 (2002) 4021–4035.

[23] R. A. Karnesky, M. E. van Dalen, D. C. Dunand, D.N. Seidman, Effects of substituting rare-earth elements for scandium in a precipitation-strengthened Al–0.08 at.

%Sc alloy, Scripta Materialia, 55 (2006) 437–440.

[24] Binary Alloy Phase Diagrams, T.B. Massalski, ed., ASM, Metals Park, OH, 1990.

[25] Y. Nakayama and H. Mabuchi, Formation of ternary $L1_2$ compounds in Al_3Ti–base alloys, Intermetallics, 1, issue 1 (1993), 41–48.

[26] S. Delsante, G. Ghosh, G. Borzone, A calorimetric study of alloys along the $Ti(Zn,Al)_3$ section, Calphad, 33, issue 1 (2009) 50–54.

[27] A. Raman and K. Schubert, Uber den Aufbau einiger zu $TiAl_3$ verwandter Legierungsreihen. I. Untersuchungen in einigen T^4-Zn-Al-, T^4-Zn-Ga- und T^4-Ga-Ge-Systemen, Z. Metallkde., 56 (1965) 40–43.

[28] G. Ghosh, A. van de Walle, M. Asta, In: Howe J, editor. Proceedings of the international conference solid–solid phase transformations in inorganic materials 2005 (PTM 2005), Warrendale, PA: TMS; 2005, vol. 2, pp. 651–656.

[29] G. Ghosh, A. van de Walle, M. Asta, First-Principles Phase Stability Calculations of Pseudobinary Alloys of $(Al,Zn)_3Ti$ with $L1_2$, $D0_{22}$, and $D0_{23}$ Structures, J. Phase Equil Diff., 28, issue 1 (2007) 9–22.

[30] N. Furushiro and S. Hori, A possible mechanism of phase transformation of Al_3Hf from Ll_2 to $D0_{22}$ during aging in a rapidly solidified Al–3Hf–0.3Si alloy, Acta Metall.,33, issue 5 (1985) 867–872.

[31] S. Srinivasan, P.B. Desch, R.B. Schwarz, Metastable phases in the Al_3X (X = Ti, Zr, and Hf) intermetallic system, Scripta Metall. Mater., 25, issue 11 (1991) 2513–2516.

[32] K. Schübert, H.G. Meissner, A. Raman, W. Rossteutscher, Einige Strukturdaten metallischer Phasen (9), Naturwiss., 51 (1964) 287.

[33] J.L. Murray, A.J. McAlister, D.J. Kahan, The Al-Hf System, J. Phase Equilibria, 19 (1998) 376–379.

[34] T. Wang, Z. Jin and J.C. Zhao, Thermodynamic Assessment of the Al–Hf Binary System, J. Phase Equilibria, 23 (2002) 416–423.

[35] K. Schübert, T.A. Anantharaman, H.O.K. Ata, H.G. Meissner, M. Pötzschke, W. Rossteutscher, E. Stolz, Einige strukturelle Ergebnisse an metallischen Phasen (6), Naturwiss., 47 (1960) 512.

[36] H. Boller, H. Nowotny, A. Wittmann, Die Kristallstruktur einiger Hafnium-haltiger Phasen, Monat. f. Chemie, 91 (1960) 1174–1184.

[37] M. M. Pötzschke and K. Schübert, Zum Aufbau einiger zu T_4-B_3 homologer und quasihomologer Systeme, Z.Metallkde, 53 (1962) 548–561.

[38] I.A. Tsyganova, M.A. Tylkina, E.M. Savitskiy, Phase diagram of the Hf–Al system, Izv. Akad. Nauk SSSR Met., 1 (1970) 160–163.

[39] J.C. Schuster and H. Nowotny, Investigations of the Ternary Systems (Zr, Hf, Nb, Ta)-Al–C and studies on complex Carbides, International Journal of Materials Research, 71 (1980) 341–346.

[40] J.C. Schuster, Document ID 20.17115.1.20, MSIT Binary Evaluation Program in MSIT Workplace, MSI Intl. Sci. Services GmbH, 2004, G. Effenberg ed, Stuttgart, Germany.

[41] S.V. Meschel and O.J. Kleppa, Standard enthalpies of formation of 5d aluminides by high-temperature direct synthesis calorimetry, J. Alloys Compd., 197, issue 1 (1993) 75–81.

[42] G. Balducci, A. Ciccioli, G. Gigli, D. Gozzi, U. Anselmi-Tamburini, Thermodynamic study of intermetallic phases in the Hf–Al system, J. Alloys Compd., 220, issue 1–2 (1995) 117–121.

[43] C. Colinet and A. Pasturel, Phase stability and electronic structure of the $HfAl_3$ compound, Phys. Rev. B 64 (2001) #205102.

[44] G. Ghosh and M. Asta, First-Principles Calculation of Structural Energetics of Al–TM (TM =Ti, Zr, Hf) Intermetallics, Acta Mater., 53, issue 11 (2005) 3225–3252.

[45] W. Rossteutscher and K. Schubert, Uber einige T–Zn- und T–Cd-Legierungssysteme, Z. Metallkd., 56 (1965) 730–734.

[46] A. Drasner and Z. Blazina, Structural Studies in the Systems $ZrZn_{2-x}Al_x$ and $HfZn_{2-x}Al_x$, Z. Naturforsch. 36b (1981) 1547–1550.

[47] G. Cacciamani, G. Borzone, R. Ferro, On a simple high temperature direct reaction calorimeter, J. Alloys Compd., 220 (1995) 106–110.

[48] G. Borzone, R. Raggio, R. Ferro, Remarks on the role of thermochemical data in intermetallic crystallochemistry, J. Alloys Compd., 367 (2004) 89–102.

[49] S. Delsante, C. Schmetterer, H. Ipser, G. Borzone, Thermodynamic investigation of the Ni-rich side of the Ni–P system, J. Chem. & Eng. Data, 55(9) (2010) 3468–3473.

[50] S. Delsante, R. Stifanese, G. Borzone, Thermodynamic Stability of RNi_2 Laves

Phases, J. Chem. Thermodyn., 65 (2013) 73–77.

[51] S. Delsante, G. Borzone, Thermochemical investigation of Sm–Mg alloys, CALPHAD, 44 (2014) 10–13.

[52] S. Delsante, R. Novakovic, A. Gagliolo, G. Borzone, Thermodynamic investigation on the Mg–Pd intermetallic phases, J. Chem. Thermodyn., 139 (2019) #105890.

[53] W. Kraus, G. Nolze, POWDER CELL – a program for the representation and manipulation of crystal structures and calculation of the resulting X-ray powder patterns, J. Appl. Crystallogr., 29 (1996) 301–303, https://doi.org/10.1107/S0021889895014920.

[54] D. Schwarzenbach, LATCON: Refine Lattice Parameters, University of Lausanne, Lausanne, Switzerland, 1966.

[55] G. Ghosh, S. Delsante, G. Borzone, M. Asta, R. Ferro, Phase stability and cohesive properties of Ti–Zn intermetallics: First-principles calculations and experimental results, Acta Mater., 54 (2006) 4977–4997.

[56] O. Levy, G. L. W. Hart, S. Curtarolo, Hafnium binary alloys from experiments and first principles, Acta Mater., 58 (2010) 2887–2897.

[57] F. N. Rhines, Phase Diagrams in Metallurgy. Their development and application., Metallurgy and Metallurgical Engineering Series, 1956, R.F. Mehl and M.B. Bever eds., McGraw-Hill Book Company, INC. New York.

[58] https://oqmd.org/materials/composition/

Figure Captions

Figure 1. SEM micrograph (BSE signal) of sample #2 in table 1. The predominant bright phase has the composition ~$Hf_{25}Zn_{75}$ and the secondary phase (dark grey) has average composition of ~$Hf_{22}Zn_{78}$. Black portions correspond to cracks and porosities.

Figure 2. Trend of the $\Delta_f H°$ (kJ/mol-atom) of the $HfAl_{3-x}Zn_x$ cubic phase as a function of *x*. A: $HfAl_3$ (TW); B: $HfZn_3$ (TW). Filled circle: $HfAl_{3-x}Zn_x$ cubic $L1_2$ ($cP4$–$AuCu_3$) phase (TW). The line AB defines the $\Delta_f H°$ of ternary alloys along the section $HfAl_3$–$HfZn_3$ assuming a mechanical mixture of DO_{23}–$HfAl_3$ and $HfZn_3$ (unknown structure).

Figure 3. SEM micrographs (BSE signal) of sample #4 in table 1. The specimen is nearly single phase having a ~$Hf_{25.0}Al_{20.5}Zn_{54.5}$ at. % composition ($HfAl_{3-x}Zn_x$ with x = 2.18). At lower magnification (3a, 500X) the presence of holes and cracks is clear.

Figure 4. SEM micrograph (BSE mode) of sample (#6 in table 1). The predominant phase has a composition ~$Hf_{25.0}Al_{24.0}Zn_{51.0}$ at. % (($HfAl_{3-x}Zn_x$ with x = 2.04). Crack and holes are present.

Figure 5. SEM micrograph (BSE mode) of sample (#9 in table 1). The specimen is single phase (grey phase) with a composition ~$Hf_{25.0}Al_{42.0}Zn_{33.0}$ at. % ($HfAl_{3-x}Zn_x$ with x = 1.32). The presence of porosities is clearly visible (black holes).

Figure 6. X-Ray diffraction pattern of the as synthesized #7 in table 1). The indexed peaks correspond to the cubic $L1_2$ phase having a ~$Hf_{25.0}Al_{31.0}Zn_{44.0}$ at. % composition ($HfAl_{3-x}Zn_x$ with x = 1.76).

Figure 7. Composition dependence of lattice parameter *"a"* of $L1_2$–$HfAl_{3-x}Zn_x$.

Table 1: Data selection of the synthesized calorimetric binary and ternary samples. The following information have been inserted: global EDS composition, calorimeter working temperature (T_c), $\Delta_f H°$ at 300K obtained by H.T. drop calorimetry, observed phases by SEM/EDS and XRPD analysis, lattice parameter of the $HfAl_{3-x}Zn_x$ cubic phase ($L1_2$). The following values of $\Delta_f H°$ (kJ/mol-atom at) of $L1_2$–$HfAl_{3-x}Zn_x$ are obtained by interpolation of our experimental data: -37.1±2.0 ($HfAl_{0.8}Zn_{2.2}$ corresponding to $Hf_{25}Al_{20}Zn_{55}$ at. %), -41.7±2.0 ($HfAl_{1.2}Zn_{1.8}$ corresponding to $Hf_{25}Al_{30.0}Zn_{45.0}$ at. %), -45.1±2.0 ($HfAl_{1.5}Zn_{1.5}$ corresponding to $Hf_{25}Al_{37.5}Zn_{37.5}$ at. %) and -48.5±2.0 ($HfAl_{1.8}Zn_{1.2}$ corresponding to $Hf_{25}Al_{45.0}Zn_{30.0}$ at. %).

#	Global EDS composition (at. %)			T_c / K (±2)	$\Delta_f H°$ kJ/mol-atom	Observed phases by XRPD and SEM/EDS analyses & comments	Lattice parameters (Å) of cubic $HfAl_{3-x}Zn_x$ phase (x value in brackets)
	Hf	Al	Zn				
1	24.5	75.5	-	1089	-37.0±2.0	Nearly one-phase sample of $HfAl_3$. Small quantity of $HfAl_2$. See text for lattice parameters determination.	
2	24.0	-	76.0	1085	-31.8±3.0	~85% of $HfZn_3$ phase and ~15% of a phase having a composition ~ $Hf_{22}Zn_{78}$ *See figure 1*	
3	25.0	15.0	60.0	1067	-35.5±2.0	Two-phase sample: cubic phase $HfAl_{3-x}Zn_x$ (x = 2.24, ~$Hf_{25.0}Al_{19.0}Zn_{56.0}$ at. %) and a phase having a composition ~$Hf_{25.0}Al_{9.0}Zn_{66.0}$ at. %	a = 4.0352(4) (x = 2.24)

4	25.5	21.0	53.5	1070	-38.2±2.0	Almost single cubic phase $HfAl_{3-x}Zn_x$ (x = 2.18, ~$Hf_{25.0}Al_{20.5}Zn_{54.5}$ at. %). *See figure 3*	*a* = 4.0362(3) (x = 2.18)
5	26.5	25.0	48.5	1067	-38.6±2.0	More than 95% of $HfAl_{3-x}Zn_x$ cubic phase (x = 2.08, ~$Hf_{25.0}Al_{23.0}Zn_{52.0}$ at. %).	*a* = 4.0367(5) (x = 2.08)
6	26.0	23.0	51.0	1070	-39.0±2.0	More than 95% $HfAl_{3-x}Zn_x$ cubic phase (x = 2.04, ~$Hf_{25.0}Al_{24.0}Zn_{51.0}$ at. %). *See figure 4*	*a* = 4.0371(3) (x = 2.04)
7	24.5	31.5	44.0	1068	-41.0±2.0	More than 95% $HfAl_{3-x}Zn_x$ cubic phase (x = 1.76, ~$Hf_{25.0}Al_{31.0}Zn_{44.0}$ at. %). *See figure 6*	*a* = 4.0392(4) (x = 1.76)
8	25.5	31.5	43.0	1065	-42.8±2.0	More than 95% $HfAl_{3-x}Zn_x$ cubic phase (x = 1.72, ~$Hf_{25.0}Al_{32.0}Zn_{43.0}$ at. %).	*a* = 4.0395(7) (x = 1.72)
9	25.5	42.5	32.0	1068	-46.0±2.0	More than 95% $HfAl_{3-x}Zn_x$ cubic phase (x = 1.32, ~$Hf_{25.0}Al_{42.0}Zn_{33.0}$ at. %). *See figure 5*	*a* = 4.0433(5) (x = 1.32)
10	25.0	47.0	28.0	1073	-52.0±2.0	Nearly single $HfAl_{3-x}Zn_x$ cubic phase (x = 1.0, ~$Hf_{25.0}Al_{50.0}Zn_{25.0}$ at. %).	*a* = 4.0450(4) (x = 1.0)

THERMOCHIMICA ACTA

Checklist for Reporting New Experimental Data

MATERIALS

1. X All studied substances (compounds and materials) must be sufficiently defined. It is advised to give at least two chemical identifiers for each compound (e.g., systematic chemical name, CAS number, structure, IUPAC PIN (Preferred IUPAC Name), InChI). In cases where complete chemical identification is impossible, sufficient information should be provided to specify the subject material.

2. NA Stereoisomers must be identified. If a mixture were used, the stereoisomeric composition should always be provided.

3. NA The manuscript needs a sample provenance table, which describes the source of all compounds used, their initial purity (if available), purification methods used, and final purity of the substance and how it was measured. The purity basis (mass, moles, volume, etc.) should be given. If abbreviated or symbolic compound names are used, they must be explained in the sample table where chemical names are given.

4. NA If a compound is hygroscopic, the water content should be determined (e.g., by Karl Fischer titration) and reported.

5. X Non-commercial compounds synthesized by the authors or others, should be properly characterized. Their chemical identity must be demonstrated (e.g., by NMR) and their final purities must be evaluated and reported.

6. NA If ^{1}H-nuclear magnetic resonance spectroscopy (NMR) is used, a graphical image of the corresponding NMR spectrum, including chemical shifts and peak integrals, must be provided in the supporting information.

METHODS

7. X Sufficient experimental details must be provided for each applied experimental method to allow the work to be reproduced by an independent researcher.

8. X In the case of new experimental set-up, the experimental method must be fully described and validated. The method validation requires comparisons with at least one well-studied system with tabulation of the validation results. In the case of existing apparatus, a summary of the method and support references must be provided, modifications to existing methods should also be described.

9. X When required, calibration details must be provided. Appropriate widely-accepted recommendations (e.g., by ICTAC or GEFTA for DSC) should be followed.

10. NA Many experimental observations are not straightforward (e.g., similar observations can be attributed to different phenomena). Therefore, what is actually seen in the experiment and how it was interpreted by the authors should be clearly identified and separated.

RESULTS

11. X It is advised that all experimental results should be collected in a single Results section (separated from Discussion) or, at least, all measured properties should be listed at the beginning of the Results and Discussion section with references to the tables and/or supplements where they are reported.

12. X All directly measured (primary) and derived property values must always be tabulated (in the main text or supporting information). The number and types of phases must be identified. Tables should be easy to parse. Excessive fragmentation of tables is discouraged. A large number of example tables have been prepared by NIST and are available (https://trc.nist.gov/TCA-Support.html).

13. X Numerical values of all state variables (e.g., pressure, temperature, compositions) must be provided together with the measured properties. The authors should consult the Gibbs phase rule for the number of state variables to be reported.

14. X Whenever applicable, numerical values for all non-state variables must be provided (e.g., frequency for speed-of-sound, electrical-conductivity, relative-permittivity measurements; wavelength for refractive-index and spectrophotometric measurements; shear rate or frequency for steady-rotation or oscillation viscosity measurements, respectively, etc.).

15. X All tables and figures must be self-explanatory. Symbols/columns/axes must be defined in headings/footnotes/captions. It is not sufficient to define the symbols in the text only.

16. X Units must always be given. SI units must be used. All compositions must be reported in mole fractions, mass fraction, or molalities. Molalities in mixtures containing three or more components require explicit definition of the solvent. If molarities, normalities, volume fractions, or other volume-based composition as well as "loadings" are used, they must be duplicated by mole fractions, mass fractions, or molalities.

17. X If SLE involves various solid forms (e.g., polymorphs, intercomponent compounds, solvates, complexes, crystals of different mixture components, etc.), experimental proof of the identity of the solid phase in equilibrium with the saturated solution is needed (e.g., via x-ray diffraction). The composition of the solid phase (e.g., the number of water molecules in hydrates) should be provided.

18. NA If solvent composition may be altered during SLE measurements (e.g., dissolution of hydrates), the contents of all components in the saturated solution should be determined and reported.

19. X Reported compositions should be clearly identified, whether they are equilibrium phase compositions, initial phase compositions, or total compositions. If the initial composition are reported, the amounts of the mixed phases should be reported (typical for gas hydrates).

20. NA Studies reporting LLE tie-lines for a ternary mixture containing two ionic compounds with different ions (e.g., ionic liquid + salt + water) must report the concentrations of all ions in each liquid phase. The same requirement is applicable for mixtures with more components.

21. X If a portion of the data has been already published by the authors (e.g., pure-component or binary endpoints), the corresponding references must be provided in the data tables to distinguish those from newly measured data.

22. X If the concept of mole is applied to intermetallic compounds, co-crystals, eutectic solvents, or other aggregates, the formula unit (entity) must be defined directly or through molar mass.

UNCERTAINTIES

23. X Uncertainties for all variables and properties (including pressure, temperature, composition) must be given in each data table and for each stand-alone (untabulated) value. In the data tables, they can be specified either in a footnote/heading or, if variable, included in the table as an additional column. See https://trc.nist.gov/TCA-Support.html for examples of acceptable uncertainty representations.

24. NA The type of uncertainty must be defined. The uncertainties should be reported as standard uncertainties u (0.68 level of confidence) or expanded uncertainties U (0.95 level of confidence). In the case of expanded uncertainties, the level of confidence must be specified. Both absolute (u, U) and relative (u_r, U_r) uncertainties are acceptable. See http://www.bipm.org/en/publications/guides/gum.html for additional details.

25. X The claimed uncertainties should be justified. The nature and origin of each contribution to the uncertainty (such as manufacturer's claim, effect of impurities, calibration, or scatter observed) should be given with an attempt to build the complete uncertainty budget. More details of Good Reporting Practice are given in the IUPAC report https://doi.org/10.1515/pac-2020-0403.

LITERATURE COMPARISON

26. X The reported experimental data should be compared with available literature data, and deviations should be discussed. If applicable, comparison for endpoints should be also included. NIST provides a literature search resource, ThermoLit (http://trc.nist.gov/thermolit), intended to aid researchers in determining relevant literature sources for a given experimental measurement. Please, note that use of ThermoLit is designed as an aid to the traditional required literature review and must not be used as a substitute.

27. X Graphical comparison should be used whenever possible.

Declaration of interests

☒The authors declare that they have no known competing financial interests or personal relationships that could have appeared to influence the work reported in this paper.

☐The authors declare the following financial interests/personal relationships which may be considered as potential competing interests: